Acoustic carrier transport in InP-based structures

M. Beck,[1,*] G. Yang,[1,†] P. V. Santos,[1,‡] and R. Nötzel[2]

[1] *Paul-Drude-Institut für Festkörperelektronik, Berlin, Germany*

[2] *COBRA Research Institute, Eindhoven University of Technology, Eindhoven, The Netherlands*

(Received April 10, 2010)

We demonstrate the ambipolar acoustic transport of optically generated electrons and holes by surface acoustic waves in InGaAsP waveguide structures grown on InP substrates. Transport is detected by monitoring the photoluminescence in the 1400–1500-nm wavelength range emitted by the recombination of the acoustically transported carriers several hundreds of micrometers away from the photoexcitation spot.

PACS numbers: 77.65.Dq, 78.55.Cr, 73.63.-b

I. INTRODUCTION

The moving strain field of a surface acoustic wave (SAW) propagating on a piezoelectric semiconductor is accompanied by a piezoelectric potential Φ_{SAW},[1] which creates moving type-II modulation of the band-gap along the SAW propagation direction. This modulation efficiently ionizes the excitons produced by incoming photons. The resulting electrons and holes are then stored in spatially separated regions close to the minima and maxima of the electronic energy -eΦ_{SAW}, respectively, which move with the well-defined acoustic velocity v_{SAW}.[2] Photons can then be retrieved if the carriers are forced to recombine by screening Φ_{SAW}. This type of acoustic charge transport (ACT) has been proposed for applications in photonic switches,[3, 4] spin,[5, 6] and exciton transport[7] as well as in the generation and detection of single photons.[8–12]

The ambipolar ACT with subsequent light emission has to date only been reported for GaAs-based semiconductors with emission wavelengths below 1 μm. In this study, we demonstrate the ambipolar acoustic transport of electrons and holes in InP-based structures emitting in the 1300–1550 nm range. By using piezoelectric ZnO layers to enhance the SAW piezoelectric fields, we show the ambipolar ACT of electrons and holes over several hundreds of micrometers as well as efficient light emission in the telecommunication range (1300–1550 nm) through the recombination of the transported carriers.

II. EXPERIMENTAL DETAILS

The studies were carried out on acoustic delay lines oriented along the [110] direction of a (001) InGaAsP layer structure grown on InP (cf. Fig. 1(a)). Each delay line consists of two aluminium split-finger interdigital transducers (IDT) designed for an acoustic

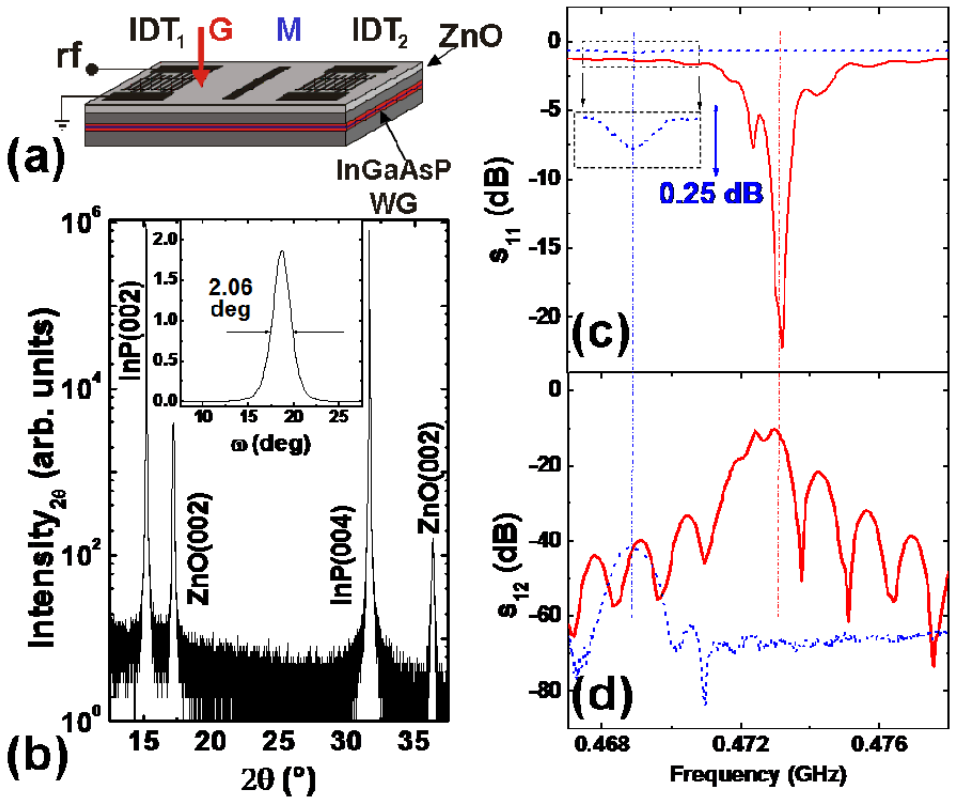

FIG. 1: (a) Schematic structure of a SAW delay line on an InAsGaP layer structure grown on InP substrates. (b) X-ray diffraction on an InP (100) substrate coated with a 500-nm-thick ZnO film. Radio-frequency (rf) power reflection coefficients (c) s_{11} and (d) s_{12} of a ZnO/InP delay line for an acoustic wavelength $\lambda_{SAW} = 5.6$ μm (solid red lines). The blue dashed lines show the corresponding coefficients in a control sample without ZnO-coating (shown expanded in the inset of (c)).

wavelength $\lambda_{SAW}$of either 4 or 5.6 μm. IDTs with a total length of 2.8 mm, aperture of 20gλ_{SAW}, and finger width of $\lambda_{SAW}/8$ were fabricated using contact lithography and lift-off metallization. Because of the weak piezoelectricity of the InP-based compounds, the acoustic excitation efficiency is very low when the IDTs are deposited directly on the InGaAsP structures (see below). We overcome this limitation by placing the IDTs over a thin (500-nm thick) piezoelectric ZnO film deposited on the semiconductor structure by radio-frequency (rf) magnetron sputtering.[13] The substrate temperature T_s, rf power, and the composition of the Ar/O_2 plasma during sputtering were optimized to yield ZnO crystallites with the wurtzite c-axis oriented along the growth direction, which ensures piezoelectricity. Best results were obtained for deposition at $T_s = 200^oC$ on surfaces previously subjected to an *in situ* Ar:N_2 ion-etch treatment. The high degree of orientation of the ZnO films is

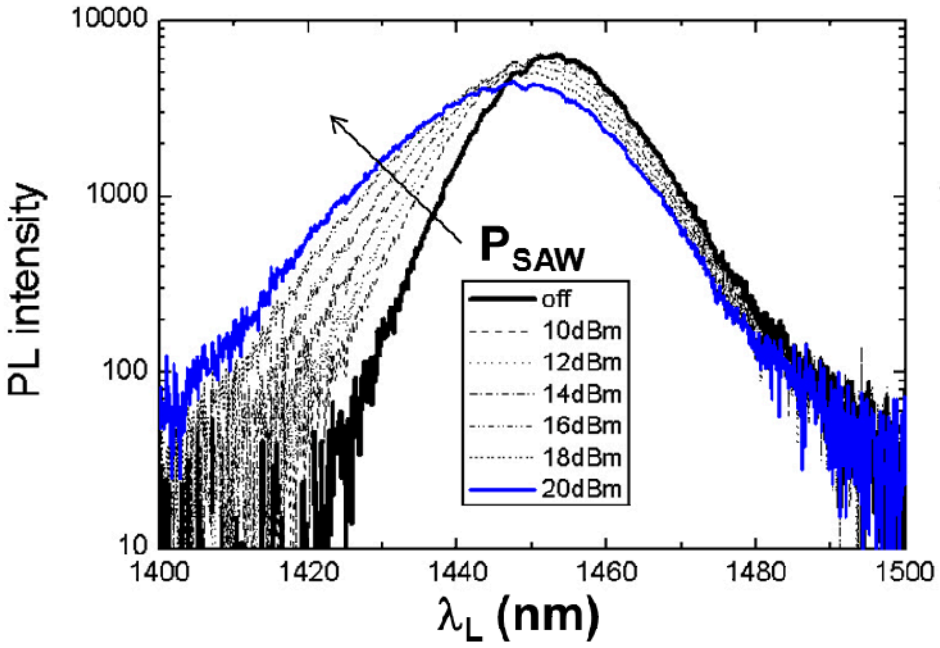

FIG. 2: Photoluminescence (PL) spectrum of the InGaAsP structures at 10 K. The PL measurements were carried out under confocal excitation and detection for different rf-power P_{SAW} applied to the acoustic transducer.

confirmed by x-ray diffraction (Fig. 1(b)), which shows only reflexes from c-oriented ZnO planes. X-ray rocking curves recorded around the ZnO (002) reflex (inset of Fig. 1(b)) have the full width at half maximum as low as 2.06^o for films grown under optimal conditions.

The improved acoustic excitation in ZnO-coated samples is demonstrated in Fig. 1(c) and (d), which show the rf power reflection (s_{11}) and transmission (s_{12}) coefficients of a delay line for $\lambda_{SAW} = 5.6$ μm on a semi-insulating InP substrate (solid red line). The blue dashed curves display, for comparison, the corresponding coefficients of a control sample without ZnO-coating. The inclusion of the ZnO film increases the s_{11} dip (which is <0.5 dB in the control sample). In addition, the transmission peak in the s_{12} coefficient becomes enhanced by approximately 30 dB. Finally, the shift of the resonance frequency (from 468.8 to 473.1 MHz) is consistent with the higher velocity of Rayleigh waves in ZnO as compared to that in InP.

The ambipolar ACT studies used spatially resolved photoluminescence (PL) to probe the carrier distribution in an InGaAsP layer structure grown epitaxially on semi-insulating InP substrates by metal-organic vapour phase epitaxy. Acoustic transport takes place in a 120-nm-thick $In_{0.74}Ga_{0.26}As_{0.44}P_{0.56}$ layer with a room temperature emission wavelength of $\lambda_{PL,RT} = 1550$ nm inserted between two 190-nm-thick $In_{0.58}Ga_{0.41}As_{0.1}P_{0.9}$ barriers with $\lambda_{PL,RT} = 1250$ nm. The whole structure was grown over a 200-nm-thick InP buffer layer

and capped by a 200-nm-thick InP layer followed by the 500-nm-thick piezoelectric ZnO film.

The PL experiments were carried out at 10 K in a microscope setup with a spatial resolution of approximately 1 μm. The carriers were photogenerated by a $\lambda_L = 675$ nm continuous wave laser focused onto an On a spot of diameter $\sim$5 μm on the SAW transport path (denoted as G in Fig. 1(a)). The PL from $In_{0.74}Ga_{0.26}As_{0.44}P_{0.56}$ emitted along the SAW path was spectrally filtered and detected using a cooled InGaAs detector array. A 120-μm-wide semi-transparent metal stripe consisting of a 6–8-nmthick Ti film was deposited over an area across the SAW path, where ZnO had been previously removed (indicated by M in Fig. 1(a) and 3(a)). This stripe quenches Φ_{SAW} and forces the recombination of the transported carriers.[2]

III. RESULTS

The black line in Fig. 2 displays the PL spectrum of the InGaAsP structure recorded at low temperatures (10 K) under confocal excitation and detection conditions using an excitation beam of approximately 30 μW placed on the SAW path. The emission is dominated by a broad (approximately 20 nm) line centered at 1450 nm. This inhomogeneously broadened PL line is attributed to potential fluctuations in the active 120-nm-thick $In_{0.74}Ga_{0.26}As_{0.44}P_{0.56}$ layer, which are probably induced by local variations in composition.

When a SAW is applied, the PL peak intensity reduces and shifts towards short wavelengths, where a pronounced tail is observed. The energetic blue shifts at this tail reach values close to 20 nm. As demonstrated below, the PL intensity reduction arises from the transport of the carriers by the SAW piezoelectric field. The energetic shifts could in principle be due to the SAW strain field, which induces a periodic modulation of the bandgap through the deformation potential mechanism, as previously demonstrated for (Al,Ga)As structures.[14] The PL energy shifts in Fig. 2 are, however, significantly larger than those expected from calculations of the strain field. In fact, by assuming a hydrostatic deformation potential $a_h = 10$ eV for the InGaAsP layers and a hydrostatic SAW strain field on the order of $s_0 = 10^{-4}$, we estimate strain-induced band gap shifts of $a_h s_0 \sim 0.1$ nm to be much smaller than those in Fig. 2.

Rather than to the strain, the blue shift under a SAW is attributed to the modification of the energetic distribution of carriers induced by the SAW piezoelectric field. In the absence of a SAW, photogenerated carriers are trapped at potential fluctuations and move by hopping, until they meet a carrier of opposite sign and recombine. The average PL energy reflects the average energy between the conduction and valence trap centers with high recombination probability. The SAW piezoelectric field enhances the emission probability of carriers trapped at the deeper centers, thereby reducing their population and increasing the average recombination energy.

The optically detected acoustic transport experiments were carried out using a delay line with two IDTs shown in the micrograph of Fig. 3(a). Figure 3(b) shows a PL image of the area in Fig. 3 (a) recorded without acoustic excitation, where light emission is only

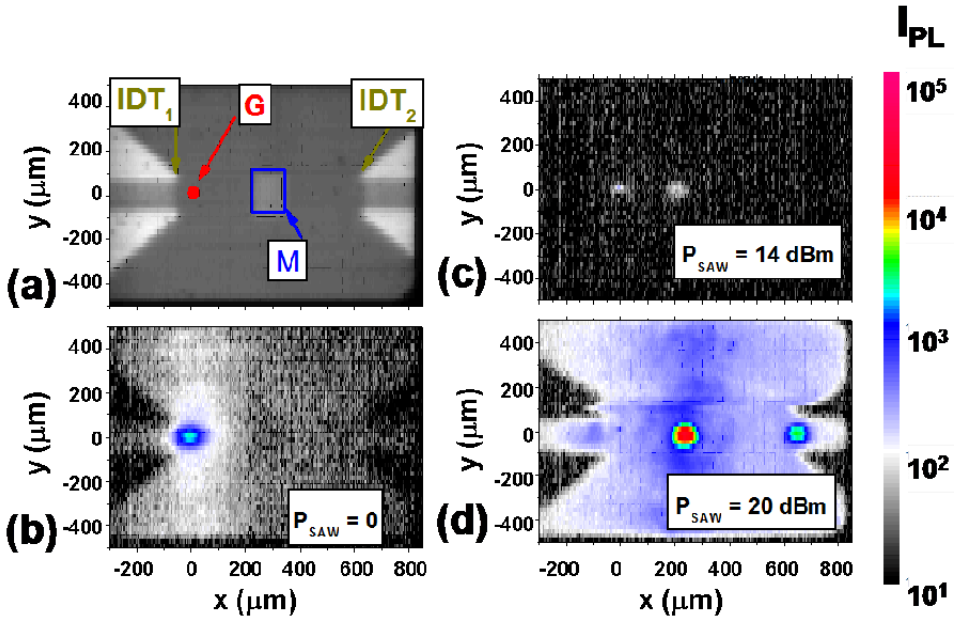

FIG. 3: (a) Optical micrograph a ZnO/InGaAsP/InP delay line for $\lambda_{SAW} = 4$ μm. (b)–(d) Photoluminescence (PL) images of the ACT recorded at 15 K for increasing rf-powers P_{SAW} applied to IDT_1 by generating carriers using a laser focused at position G in (a). M denotes a semi-transparent metal layer used to block the acoustic transport and induce carrier recombination. For high acoustic power, PL is also observed at the input of the opposite (unpowered) transducer IDT_2.

observed close to the laser spot G at x= 0. The PL close to G reduces with the nominal acoustic power (P_{SAW}) applied to IDT_1, as illustrated in Fig. 2(c) (the second IDT of the delay line (IDT_2) was kept unpowered in all experiments). The reduction is attributed to the spatial separation and transport of the photogenerated electrons and holes away from G by the SAW piezoelectric field, as previously observed for GaAs [2]. The PL is retrieved as the carriers recombine close to the metal stripe M. For higher acoustic powers (Fig. 3(d)), the emission at M increases significantly while the one at G practically disappears. In addition, PL emission is also observed at the entrance of IDT_2 at a distance exceeding 500 μm from G. The latter is attributed to the fact that the field screening by the metal layer becomes inefficient under high acoustic intensities so that the carriers can still be transported underneath the metal stripe and can reach the opposite IDT. The small size of the recombination spots shown in Figs. 3(c) and 3(d) arises from the fact that the piezoelectric potential keeps the carriers within the acoustic beam, thus preventing their lateral diffusion during the transport.

It is interesting to note that under strong acoustic excitation the remotely detected PL at M (cf. Fig. 3(d)) is much stronger than the one detected at the generation spot G in the absence of acoustic excitation (cf. Fig. 3(b)). This effect becomes evident in Fig. 4, which compares PL profiles integrated along the beam cross-section (y-direction)

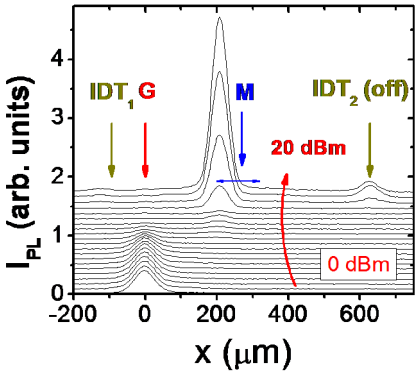

FIG. 4: Integrated PL profiles along the SAW transport path for different nominal rf-powers (P_{SAW}) applied to IDT$_1$ (cf. Fig. 2(a)). P_{SAW} was varied in steps of 1 dBm from 0 (lowest curve) to 20 dBm (highest curve).

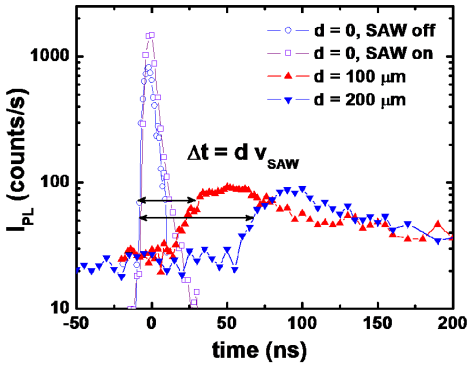

FIG. 5: Time-resolved PL traces recorded Under excitation by means of a pulsed laser beam for different distances d between the generation (G, cf. Fig. 3(a)) and detection (M) spots.

for different P_{rf}. For the highest applied power, the PL intensity at M exceeds that at G by almost one order of magnitude. This behavior, which has not been previously observed in GaAs structures,[2, 3] indicates that the SAW fields substantially increase the radiative recombination probability in the $In_{0.74}Ga_{0.26}As_{0.44}P_{0.56}$active layer. As previously discussed in connection with Fig. 2, the dynamic character of the SAW field reduces the average population of deep traps as compared to the shallow ones, which are expected to have a shorter radiative recombination lifetime.

To demonstrate that the carriers are actually transported at the SAW speed v_{SAW}, we have carried out time-resolved studies of the transport process using pulsed laser excitation (consisting of 100-ps pulses with a wavelength of 675 nm and a repetition rate of 20 MHz) and time-gated detection (Fig. 5). The open symbols display time-resolved PL traces for confocal illumination and detection in the absence (squares) and presence (cycles) of a SAW, respectively. In both cases, the PL decay time is comparable to the experimental time resolution. The solid symbols display the PL recorded at the edge of the metal stripe M for remote light excitation at distances d= 100 μm and d= 200 μm away from M. The delayed PL response is well accounted for by the expected SAW propagation times $\delta t = d/v_{SAW}$ of 38.2 and 76.2 ns, respectively, from the generation to the detection positions (the expected propagation times are indicated by the length of the arrows). Note, in addition, that the decay time of the remote PL is much longer than the confocal one, thus indicating that the many carriers take much longer times to arrive the detection point. The long decay is attributed to the capture and subsequent re-emission of carriers by trapping states along the SAW path, which reduces the effective transport velocity.

IV. CONCLUSIONS

In conclusion, we have demonstrated the efficient generation of SAW beams as well as optically detected ambipolar transport of electrons and holes in InGaAsP structures. The results presented here open the way for acoustically driven acousto-optic devices operating at telecommunication wavelengths.

Acknowledgments

We thank M. Ramsteiner for comments and for a critical reading of the manuscript as well as B. Drescher and W. Seidel for sample fabrication. The support of the European Network of Excellence ePIXnet and ACDET-Project is gratefully acknowledged.

References

* present address : Faculty of Science and Technology, University of Twente, Enschede, The Netherlands
† present address : Wuhan National Lab. for Optoelectronics, Huazhong University, Wuhan, China
‡ Electronic address: santos@pdi-berlin.de

[1] N. J. Moll, O. W. Otto, and C. F. Quate, J. Phys. Colloq. (France) **33**, 231 (1972).
[2] C. Rocke *et al.*, Phys. Rev. Lett. **78**, 4099 (1997).
[3] F. Alsina, J. A. H. Stotz, R. Hey, and P. V. Santos, Solid State Commun. **129**, 453 (2004).
[4] V. I. Talyanskii, M. R. Graham, and H. E. Beere, Appl. Phys. Lett. **88**, 083501 (2006).
[5] J. A. H. Stotz, R. Hey, P. V. Santos, and K. H. Ploog, Nat. Mater. **4**, 585 (2005).
[6] F. Iikawa *et al.*, Phys. Rev. Lett. **95**, 077203 (2005).
[7] J. Rudolph, R. Hey, and P. V. Santos, Phys. Rev. Lett. **99**, 047602 (2007).
[8] C. Wiele, F. Haake, C. Rocke, and A. Wixforth, Phys. Rev. A **58**, R2680 (1998).
[9] C. L. Foden *et al.*, Phys. Rev. A **62**, 011803(R) (2000).
[10] V. I. Talyanskii, G. J. Milburn, J. A. H. Stotz, and P. V. Santos, Semicond. Sci. Technol. **22**, 209 (2007).
[11] P. D. Batista *et al.*, Appl. Phys. Lett. **92**, 133502 (2008).
[12] O. D. D. Couto, Jr. *et al.*, Nat. Phot. **3**, 645 (2009).
[13] C. S. Tsai, B. Sun, and A. Kar-Roy, Appl. Phys. Lett. **70**, 3185 (1997).
[14] T. Sogawa *et al.*, Phys. Rev. B **63**, 121307(R) (2001).